Structures 55 (2023) 1159–1171

Contents lists available at ScienceDirect

Structures

journal homepage: www.elsevier.com/locate/structures

Structural behavior of steel tie connections in masonry veneer walls: Proposal of a simplified approach for practice

Javier Ortega [a,b,*], Nuno Mendes [b], Graça Vasconcelos [b]

[a] Instituto de Tecnologías Físicas y de la Información "Leonardo Torres Quevedo", Consejo Superior de Investigaciones Científicas (CSIC), C/Serrano 144, 28006 Madrid, Spain

[b] University of Minho, ISISE, ARISE, Department of Civil Engineering, Guimarães, Campus de Azurém, 4800-058 Guimarães, Portugal

ARTICLE INFO

Keywords:
Brick masonry
Veneer walls
Steel ties
Tension–compression behavior
Finite element modeling
Numerical analysis
Spring model
Experimental analysis
Structural design

ABSTRACT

Steel ties perform a key structural role in ensuring the stability of buildings façades built with brick masonry veneer walls. These elements are responsible for transferring the loads acting on the veneer wall to the main structure, which typically consists of masonry infill walls used in reinforced concrete frames buildings. Such constructive system is common in Portugal and other Mediterranean countries where the seismic hazard is high. In the event of an earthquake, the ties have to transfer the out-of-plane loads and are subjected to significant tension and compression stress. The characterization of the seismic behavior of these tie connections is an insufficiently explored topic. Despite the codes available for the design of brick masonry veneers and ties, recent earthquakes brought to light the seismic vulnerability of this constructive system. The present paper proposes a simplified spring numerical model validated with experimental results. The simplified model can be applied to perform numerical analyses of greater scale (e.g. to analyze full façades of buildings), which can help to optimize the design. Finally, the paper identifies a common construction problem, which is the probable misalignment of the mortar joints of the masonry walls. A construction solution is proposed by the authors.

1. Introduction

Brick masonry veneer walls are essentially a type of cavity wall consisting of an exterior cladding acting as a skin of the structure and separated from it by an air cavity, which is often filled or partially filled with insulation material. The masonry veneer walls serve the buildings as an aesthetic element and can act as barriers to moisture penetration. The air cavity allows air ventilation between leaves, improving the thermal efficiency of buildings. The veneer leaf is anchored to the backing system through ties and supported vertically by the floor slabs, by shelf angles located at each floor, or directly by the foundations. The veneer should transfer out-of-plane load directly to the backing structure and is not considered to add load-resisting capacity to the wall system. Veneer walls offer a good performance in terms of aesthetics, durability and thermal behavior and that is the reason why their use spread in several countries in the world during the last 50 years. This constructive solution can also be applied in the renovation of traditional façades to improve the energy efficiency of existing buildings.

There are distinct types of ties connecting the brick masonry veneer walls to the backing system [25,26], generally made of steel and with a variable geometry. The main role of wall ties on masonry veneer walls is transferring the lateral loads (e.g. wind or seismic loads) to the backing structure, providing a connection between both. For a tie to be effective it must: (i) have enough stiffness to transfer lateral loads with minimal deformations; (ii) have mechanical resistance; (iii) have shear flexibility to accommodate in-plane movements; (iv) be corrosion-resistant; and (v) be easily installed to reduce installation errors [7,8]. The connectors should be also selected according to the type of structural and backing system, and the local seismic hazard [8]. Commonly, wire and corrugated ties have been used for masonry veneers coupled with loadbearing and non-loadbearing masonry and concrete walls. There are several recommendations for the design and detailing of wall ties available in different codes [27,28,1,9], typically ranging from 2 to 5 ties per square meter. Eurocode 6 [16] indicates that, in the case of cavity walls, the number of ties under lateral loads should be defined according to the level of lateral load applied on the wall. Additionally, in cavity and veneer walls subjected to lateral wind loads, the wall ties connecting the cavity leaves or the veneer to the backing system shall be capable of distributing the wind loads from the loaded external leaf to the internal leaf and from the veneer wall to the backing system, respectively.

* Corresponding author.
E-mail address: javier.ortega@csic.es (J. Ortega).

https://doi.org/10.1016/j.istruc.2023.06.077
Received 13 December 2022; Received in revised form 3 May 2023; Accepted 14 June 2023

Nevertheless, some recent earthquakes brought to light some fragilities of this constructive system, resulting in damages due to combined in-plane and out-of-plane loads, namely extensive diagonal cracking and out-of-plane detachment from the backing support [20,11,21]. Despite the significant influence of veneer walls on the dynamic response of the building under seismic actions [24,19] and their obvious structural role, they are still considered as a façade element. As a result, there are no specific regulations for the design of brick masonry veneers and ties.

Research works dealing with the seismic behavior of veneer masonry walls have mostly focused on structural systems consisting of timber or steel frames [37,39,32,18,29,30,31]. These works highlighted already some aspects that are particularly influential on the seismic behavior of brick veneers, namely the tie connection spacing and stiffness, the relative stiffness between the facing and backing structure, the support conditions of brick veneer and the backup, the location of wall edges and openings, the air cavity width, and the type of loading applied to the wall [7]. The backing structure has thus been identified as a key factor, which manifests the need to conduct research on the seismic performance of masonry veneer walls attached to different backing systems, with the objective of developing suitable design approaches. The present research focuses on veneer walls attached to reinforced concrete frames with masonry infill walls, which is the most common backing structural system in Portugal and other European countries. The main objective is to develop a simplified approach for practitioners that can eventually aid in the seismic design and detailing of brick masonry veneer walls and the necessary tie connections.

The content of the present paper is structured into six sections. After the introduction, the second section introduces the experimental campaign that was carried out to characterize the tension–compression behavior of tie connections in masonry veneer walls, when the ties are located in the mortar joints. The wide experimental campaign helped to obtain a better understanding of the most influential parameters on the structural behavior of the tie and failure modes. The third section presents the proposed simplified numerical approach. A simplified numerical spring model with nonlinear elasticity was developed, defined by distinct loading and unloading stiffness diagrams. The fourth section deals with the validation of the simplified spring model, using experimental results from different types of ties. It can eventually be applied for design purposes. It is noted that estimating the action that goes to each tie is difficult. Thus, the use of the proposed simplified spring model on numerical analyses of greater scale, e.g. aimed to analyze major structural components or buildings, allows estimating the load acting on each tie more precisely and can help to optimize the structural design.

Finally, the fifth section of the paper discusses a common problem typically encountered during the construction of masonry veneer walls, namely the probable misalignment of the mortar joints of the facing and backing masonry walls. Adapted from an existing solution from the market, the paper proposes a new solution that helps to solve the misalignment without reducing the capacity of the tie because of the eccentricity in the application of the load. The proposed solution is validated with numerical analysis and a simple analytical expressions are also provided for design and assessment. The paper ends with the main conclusions of the present work.

2. Experimental characterization of tie connections

An extensive experimental campaign was carried out to characterize the tension–compression behavior of ties in veneer masonry walls [22]. This experimental characterization served as a basis for the selection of a simplified approach to simulate the structural behavior of the ties connecting veneer walls that can be applied in practice for design purposes. The reader is referred to [22] for a detailed discussion of the experimental campaign. In summary, ties embedded in the mortar bed joints in different brick masonry wallets were subjected to cyclic tension–compression tests to evaluate their bond resistance. Three test specimens were built (Fig. 1): (a) prisms representative of common brick masonry infill walls used in Portugal; (b) prisms representative of common brick masonry veneer walls used in Portugal; and (c) complete assemblages with brick masonry veneer prisms attached to brick masonry infill prisms through ties. In the complete assemblages, an air cavity thickness of 100 mm was considered.

The mechanical properties of brick and mortar of the different masonry specimens were also characterized experimentally [22,34,35,2,3]. In terms of geometry, the veneer prisms are built with ceramic bricks with vertical holes and approximately 237 mm × 115 mm × 70 mm (length × thickness × height). The masonry infill prisms are built with brick units with horizontal perforation and approximately 300 mm × 150 mm × 200 mm (length × thickness × height). The average compressive strength is 24 MPa and 4 MPa for the veneer and infill brick unit, respectively. The average values of compressive strength of the cement mortar were 5.2 MPa and 6.9 MPa for the veneer and infill prisms, respectively. The mortar bed joint thickness of both prisms is 15 mm. With respect to the ties, the experimental campaign included several types of different geometries (Fig. 2). T1 has a U-shaped cross-section in the central part and the two extremes have a complex anchorage shape. T2 is a steel ribbed bar, T3 is a steel bar with twisted ends, T4 is also a steel bar that ends in a hook shape, and T5 is a plain-ended basalt fiber tie. All ties are anchored within the mortar bed joint embedded 60 mm in the infill brick masonry prism and 65 mm in the veneer masonry prism.

The experimental setup consisted of confining vertically the masonry prisms and then applying horizontal tension–compression displacements with cycles of increasing amplitude. Fig. 3 shows a summary of the experimental results obtained in terms of average load–displacement diagram for the complete assemblages with tie type T1 (Fig. 3a) and monotonic envelopes for the different types of specimens (Fig. 3b). The most common failure modes observed were sliding of the tie within the mortar, combined sliding-cone failure of the mortar surrounding the tie, tie buckling and tie fracture. Typically, the maximum tensile load corresponds to the pull-out of the tie from the mortar joint, while the maximum compressive load is associated to tie buckling.

3. Simplified numerical approach

The simplified spring model proposed in the present research is intended to be applied in numerical analyses of greater scale, e.g. aimed to analyze major structural components (full façades) or buildings. The idea behind developing a simplified spring model is that practitioners can use it to assess the structural performance of the ties under out-of-plane loading. The model should be simple (ideally easy to apply in any commercial structural analysis software) and should require low computation effort. Therefore, the approach can help in the design of the solution.

Detailed numerical models able to simulate all possible failure modes observed during the experimental tests may require the modeling of the tie, the discretization of the masonry into the two constituents (brick and mortar), interface elements between the tie and the mortar, etc. Such detailed models require that some of the elements have dimensions around the millimeter and thus have a high computational demand. Previous works aimed to simulate the experimental tests [33] resulted in models with a total of 18,086 elements and 10,465 nodes and it only simulates 4 bricks, making it inappropriate to be used for a whole building. Therefore, the simplified model aims to find a compromise between the accuracy of the more detailed numerical models and computational demand.

The present section firstly presents the modeling approach proposed, consisting of a spring model with nonlinear elasticity defined by distinct loading and unloading stiffness diagrams. Secondly, it defines the analytical procedure proposed to define the stiffness diagram. Finally, it shows a comparison of the results obtained in the simplified model,

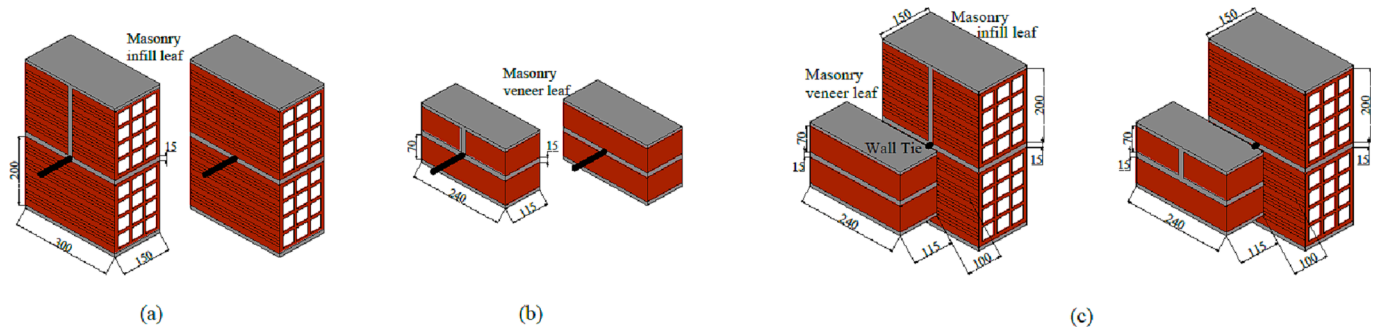

Fig. 1. Test specimens: (a) brick masonry infill with embedded tie; (b) brick masonry veneer with embedded tie; (c) complete assemblage of brick masonry prims connected [22].

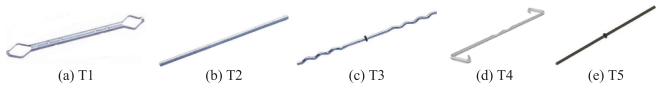

Fig. 2. Wall tie typologies used in the experimental campaign [4].

defined by the analytical stiffness diagram, with the results from the experimental parametric analysis performed by [22]. This comparison involves different tie geometries and variations in the embedment length, types of mortar and cavity thickness.

3.1. Simplified spring numerical model: concept and assumptions

The proposed spring model was first numerically tested. Fig. 4 shows the idea behind the new simplified numerical model prepared to simulate the complete assemblage of the two brick masonry prisms connected with the tie (Fig. 1c). The simplified numerical model consists simply of one spring element and the two masonry prisms, which are not discretized into brick and mortar and have the homogenized properties of the masonry (macro-modeling approach). The discretization of the masonry can be more or less coarse depending on the objective and type of analysis. The numerical model presented in Fig. 4 is meant to serve as an example and has 3,150 elements and 4,033 nodes. When the masonry is considered as an elastic material, as in the following analysis that is only focused on the behavior of the tie, the model can be further simplified. For analyses that take into account the nonlinear behavior of the masonry, the mesh can be further refined.

The model was prepared in DIANA [38] and the spring element is a two-node spring element (SPT2R element type in DIANA). A nonlinear elasticity model was assigned to the spring, allowing to define a multilinear spring stiffness diagram, including the loading/unloading/reloading behavior. In DIANA, one diagram is defined for tension and another for compression.

To define the loading/unloading/reloading diagrams in DIANA, the experimental curves were simplified into a four-linear force–elongation diagram: (1) the first loading branch corresponding to the elastic stiffness of the tie; (2) the second plateau branch corresponding to the maximum load obtained (zero stiffness); (3) the unloading linear softening branches corresponding to the strength degradation after peak load; and (4) the fourth branch corresponding to the plateau describing the residual strength of the tie, which initially was considered as 0 (no residual strength). Fig. 5 shows the diagrams defined to obtain the four-linear force–elongation diagram that matches well the experimental results of the complete assemblage with tie type T1 (hereinafter the reference model). It is noted that an ultimate force was defined for each diagram, namely 3 kN for the loading diagram and 2.5 kN for the unloading diagram.

After the diagram was implemented, a numerical analysis was run to verify that the model behaves as expected. Several loading/unloading cycles were imposed on the model. Fig. 6 shows the results of the analysis. The defined diagrams reproduce effectively the tension–compression behavior of the tie implemented with the diagram shown in Fig. 5a. One of the simplifications that had to be assumed for the defined spring model is that the pinching effect and the crack closure cannot be reproduced. The deformation in the numerical model is permanent. When the load is reverted from tension to compression (and vice versa), the model changes the diagram (loading–unloading) and applies the corresponding stiffness defined in Fig. 5a for that displacement (x-axis). The stiffness is constant until reaching the ultimate load and the second plateau branch with zero stiffness. Thus, the proposed

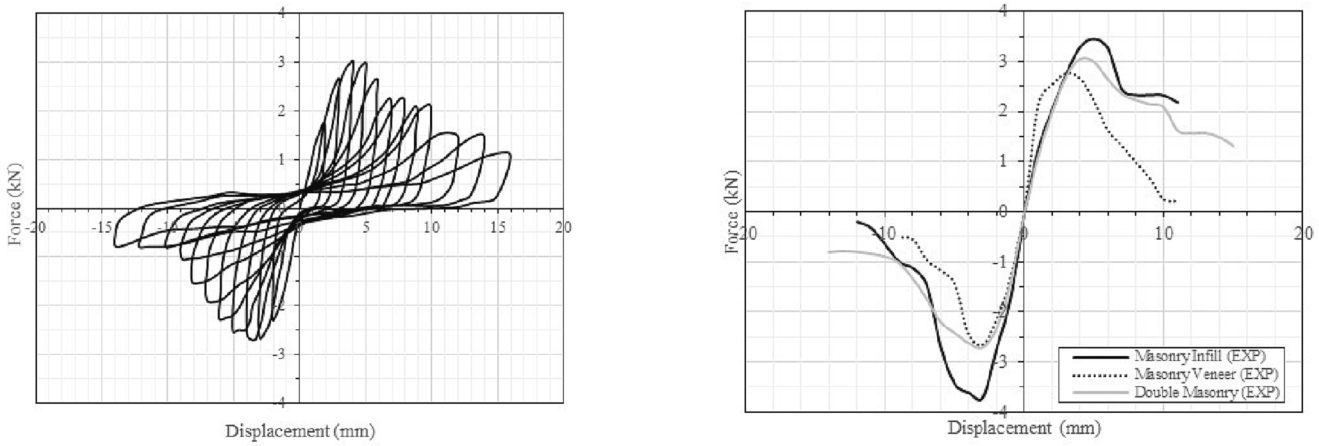

Fig. 3. Cyclic tension–compression tests results for the complete assemblage specimen: (a) load–displacement diagram; (b) monotonic envelope curves from cyclic tests; adapted from [22].

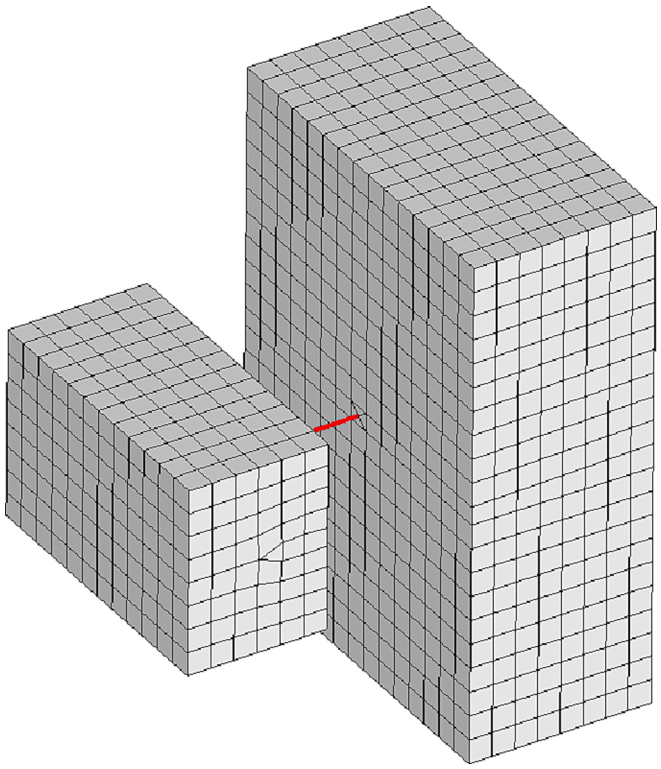

Fig. 4. Simplified numerical model developed with the spring element connecting the two masonry prisms.

simplified modeling approach is mainly recommended for nonlinear static analysis (pushover analysis, which correspond to the most used type of analysis for seismic assessment), avoiding possible non-conservative results for the nonlinear dynamic analysis, due to an overprediction of the energy dissipated by the ties. In addition, and for an even simpler approach, the proposed simplified modeling can be also used for linear static and dynamic analysis, simulating the linear stiffness of the ties by the springs and comparing, at the end of the analysis, the maximum applied forces at the ties with the strength of all failure modes.

3.2. Definition of the spring constitutive model

The development of the simplified spring model to simulate the tension–compression behavior of the tie requires the definition of the four-linear force–elongation diagram. The definition of the diagram will depend on material properties (tie and masonry), geometric and construction parameters that influence the structural behavior of the assemblage, namely the mortar material properties, the cavity thickness, the tie length (i.e. tie buckling) or embedment length. As was observed during the experimental tests, these parameters clearly influence the capacity of the assemblage and the failure mode observed.

The linear branches of the diagram can be defined according to simple analytical formulas, depending on the most probable failure modes observed in the experimental analysis. The diagrams obtained are firstly validated with the reference experimental analysis. Then, a parametric analysis is carried out to verify if the methodology established to define the diagram works well for the different situations that were studied experimentally.

3.2.1. Definition of the maximum load

The most common failure modes reported by [22] during the experimental campaign and similar research works [17,5,6,10,36] are: (1) tie fracture; (2) sliding failure; (3) cone failure; (4) combined cone and sliding failure; (5) buckling failure; and (6) piercing and expulsion of the mortar failure. Note that the failure modes considered refer to ties embedded in the mortar joint, which is the location of the ties considered in the present study, thus excluding those failures associated with ties embedded in brick units, e.g., masonry unit splitting or masonry unit pull-out. Analytical models can be applied to define the maximum load corresponding to all six considered failure modes, which can be used to define the maximum load that the tie can resist in both tension and compression.

3.2.1.1. Tie fracture. This failure mode is controlled by the tensile strength of the tie. The maximum load that the tie will stand before it fractures is given by the formula:

$$N_{max} = Af_y \tag{1}$$

where A is the cross-section area, A, and f_y is the yield strength of the steel (i.e., tie material).

3.2.1.2. Tie sliding. The formula that can be used to define the maximum force corresponding to the tie sliding is based on the shear breaking of the interface between the tie and the mortar or brick where

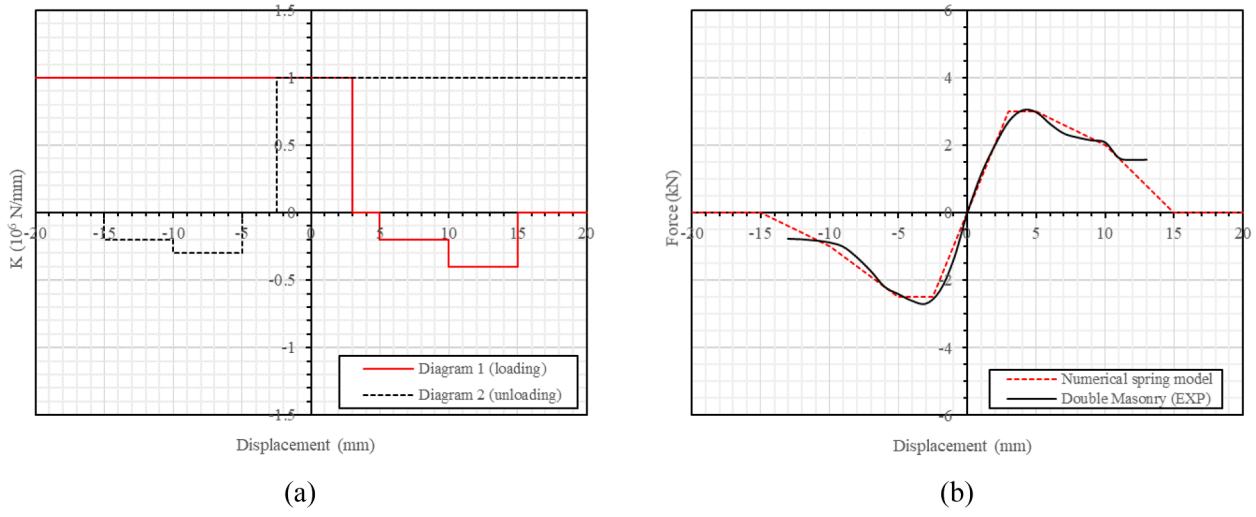

(a) (b)

Fig. 5. (a) Loading and unloading diagrams defined for the spring element; (b) expected four-linear force–elongation curve that simulates the experimental results.

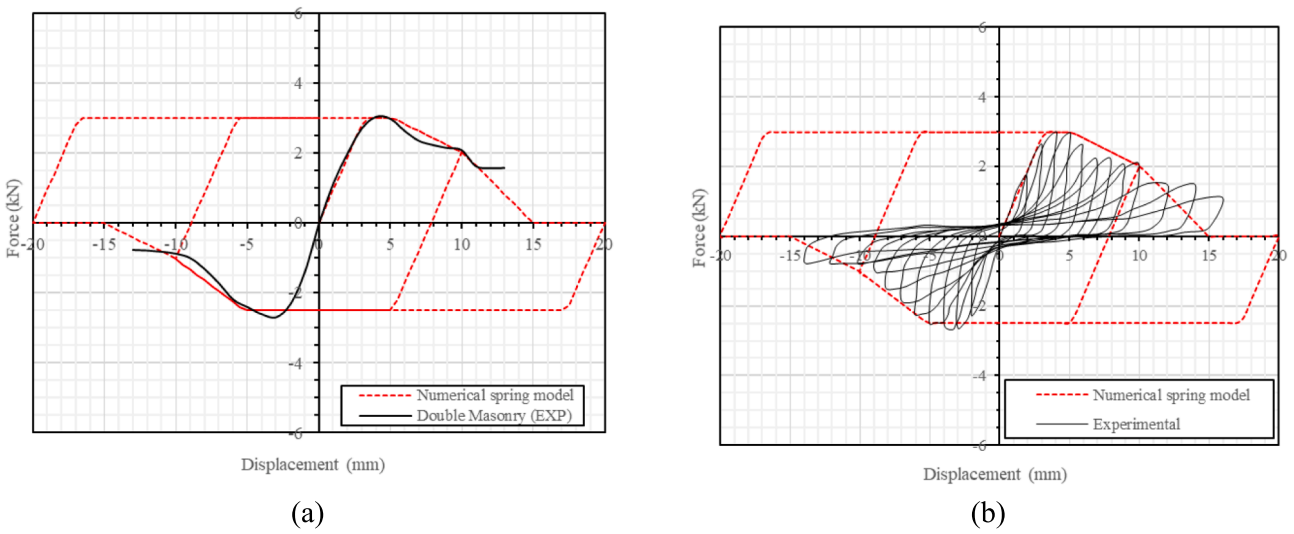

Fig. 6. Comparison between the numerical results obtained using the spring model with no residual strength and the experimental results: (a) monotonic envelope; and (b) cyclic loading.

it is embedded [23]. In this case, the pull-out capacity is given by:

$$N_{max} = \tau_{max} p_0 h_{ef} \tag{2}$$

where τ_{max} is the maximum shear stress at the interface, p_0 is the perimeter of the cross-section and h_{ef} is the embedment length of the tie. Thus, the values of $p_0 h_{ef}$ results in the contact area between the tie and the mortar. The maximum shear stress at the interface (τ_{max}) defining the sliding failure highly depends on the adherence and shear resistance of the mortar (or embedding medium). In the literature, some studies propose to consider the tensile strength of the embedding medium as the maximum shear stress [12]. In this case, the value is calibrated numerically [33]. This study assumed a cohesion value of 1.1 MPa at the mortar-tie interface to match the experimental load–displacement curve.

3.2.1.3. Cone failure. The maximum force governing the cone failure can be defined using the common concrete cone model [14], which primarily depends on the embedment length of the tie:

$$N_{max} = 0.92 {h_{ef}}^2 \sqrt{f'} \tag{3}$$

where f' is the compressive strength of the mortar (or the material where the tie is embedded.

3.2.1.4. Combined sliding and cone failure. This failure considers the possibility of a combined mechanism given by a shallow mortar cone failure with sliding at the tie-mortar interface below the cone [13]:

$$N_{max} = \tau_{max} p_0 h_i + 0.92 (h_{ef} - h_i)^2 \sqrt{f'} \tag{4}$$

where h_i is the sliding length and h_{ef} is the depth of the cone. To apply this formulation, it is necessary to find the sliding length that will lead to the lowest maximum load that will lead to the combined mechanism.

3.2.1.5. Buckling failure. The buckling failure was at first evaluated analytically for the reference model, which has a cavity thickness of 100 mm. The aim was to determine the critical load (P_{cr}) that would make the tie become unstable and buckle. The critical buckling load is given by the Euler formula:

$$P_{cr} = \frac{\pi^2 EI}{(KL)^2} \tag{5}$$

where E is the modulus of elasticity of the material (steel), I is the moment of inertia in the orthogonal direction to the direction of buckling, L is the length of the slender element, and K is the effective length factor, which depends on the support conditions of the element. Common values are: 0.5 (fixed–fixed ends), 0.7 (pin-fixed ends), 1 (pin-pin ends) and 2 (fixed-free ends). For the reference model, L was assumed as 100 mm, and the support conditions should be somewhere between 0.5 and 1 since it cannot be considered neither as a rigid or a pinned connection. The modulus of elasticity assumed for the steel is 200 GPa and the moment of inertia is calculated for the weaker direction (I_x = 31.2 mm^4). Given the abovementioned characteristic, Eq. (5) results in a value of critical load (P_{cr}) ranging between 6.1 kN ($K = 1$) and 24.6 kN ($K = 0.5$), and 12.6 kN for $K = 0.7$.

Aiming at understanding the influence of the cavity thickness on the tension–compression behavior of the tie connection, the cavity thickness was increased, increasing the proneness to buckling failure. This failure mechanism was commonly observed in the experimental cyclic tension–compression tests carried out by [22]. Four extra configurations were analyzed varying the free length of the tie (equal to the cavity thickness) but keeping the embedment length in each masonry fixed, i.e. 65 mm within the infill masonry prism and 60 mm within the veneer masonry prism. Thus, the cavity thickness increases and decreases according to the variations of the tie length.

Table 1 shows the variations of the critical buckling load (P_{cr}) according to the cavity thickness considered and for three different K values (0.5, 0.7 and 1.0). Table 1 shows that the only two configurations that would yield values close to the maximum load obtained experimentally (2.7 kN) correspond to the tie length of 275 or 300 mm and the connection is considered a pin-pin connection.

Even though the experimental results proved that the tie is prone to buckling, the previous results show that the tie should not buckle under the considered conditions. Therefore, the buckling may be attributed to possible imperfections of the material and/or eccentricities in the load application. This possibility was also explored following the approach defined by the Eurocode [15], which states that a compression member should verify that:

$$\frac{N_{Ed}}{N_{b,Rd}} \leq 1.0 \tag{6}$$

where N_{Ed} is the design value of the compression force and $N_{b,Rd}$ is the design buckling resistance of the compression member, which can be

Table 1
Variations of the critical buckling load (P_{cr}) according to the tie length.

Tie length (mm)	200			225 (Ref)			250			275			300		
Cavity thickness (mm)	75			100			125			150			175		
K	1.0	0.7	0.5	1.0	0.7	0.5	1.0	0.7	0.5	1.0	0.7	0.5	1.0	0.7	0.5
P_{cr} (kN)	10.9	22.3	43.7	6.1	12.6	24.6	3.9	8.0	15.7	2.7	5.6	10.9	2.0	4.1	8.0

calculated as:

$$N_{b,Rd} = \frac{\chi A f_y}{\gamma_{M1}} \tag{7}$$

where χ is the reduction factor for the relevant buckling mode, A is the cross-section area of the member, f_y is the yield strength of the steel and γ_{M1} is a particular partial factor that can be assumed as 1.0 (recommended values for buildings in the Eurocode). The reduction factor can be determined from the buckling curves specified in the code as:

$$\chi = \frac{1}{\phi + \sqrt{\phi^2 - \bar{\lambda}^2}} but \chi \leq 1.0 \tag{8}$$

where the buckling curve is defined by:

$$\phi = 0.5\left[1 + \alpha(\bar{\lambda} - 0.2) + \bar{\lambda}^2\right] \tag{9}$$

where α is an imperfection factor that depends on the type of cross-section (see below) and λ is the non-dimensional slenderness that can be computed as:

$$\bar{\lambda} = \sqrt{\frac{A f_y}{N_{cr}}} \tag{10}$$

where N_{cr} is the previously defined critical buckling load (P_{cr}), calculated using the Euler formula (Eq. (5). It is noted that, to be on the safe side, a K of 1.0 was adopted in the calculations, assuming a pinned connection. This leads to a critical load for the reference model of 6.1 kN (Table 1).

Following the code indications and using an imperfection factor (α) of class c (0.49), the resulting $N_{b,Rd}$ is 2.57 kN. Note that a class c is assigned to U-section profiles such as the one considered for the analysis. This value is close to the maximum value obtained experimentally, which shows that the tie is indeed prone to buckling for the range of load imposed during the tension–compression tests and justifies the buckling failure modes observed during the experimental campaign. Fig. 7 shows how the maximum compression load obtained during the experimental analysis is only slightly over the resulting buckling load calculated taking into account possible imperfections of the system.

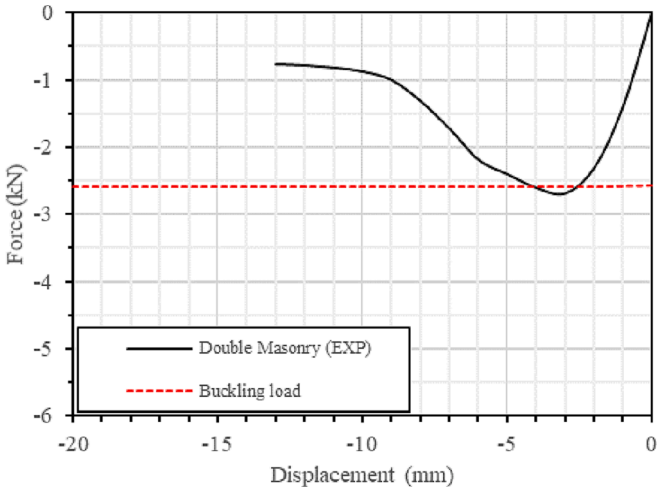

Fig. 7. Comparison between buckling load and experimental results for the complete assemblage.

As a summary, the load leading to buckling failure can be calculated using the procedure described considering imperfections of the material and/or eccentricities in the load application, i.e. using Eq. 5–10.

3.2.1.6. Piercing and expulsion of the mortar failure. This failure consists of the piercing and expulsion of the cone of mortar around the tie according to what was reported by [5,6]. This failure mainly occurs under compression and it is a combination of sliding at the tie-mortar interface with the expulsion of the cone of mortar behind the tie. The activation of the mortar behind the tie increases the capacity of the system with respect to a pure sliding failure type that occurs under tension loading. This failure was also particularly important for ties with a hook that is able to activate a notable amount of mortar surrounding the tie under compression when the tie is subjected to tension loading.

There are no specific analytical formulas in the literature to quantify the maximum load governing this failure, but a new one is proposed based on the cone concrete failure type, assuming a common diagonal 45-degree failure surface (Fig. 8). A uniform stress distribution acting normal to the inclined failure surface is assumed. However, instead of a cone, the failure is considered to occur only at the joint. Thus, the failure surface is composed of two vertical diagonal stripes taking an inclination of 45° from the tie.

The tensile stress distribution used is the same as proposed in the concrete cone model ($f_t = 0.33\sqrt{f'}$). The assumed stress distribution leads to the following maximum capacity:

$$N_{exp,mortar} = 0.67 d h_j \sqrt{f'} \tag{11}$$

where d is the depth of the mortar from the end of the tie until the end of the brick and h_i is the thickness of the joint. Since the failure mode is a combination of the expulsion of the mortar and the sliding of the tie, the complete formula that can be used to define the failure mode reads:

$$N_{max} = 0.67 d h_j \sqrt{f'} + \tau_{max} p_0 h_{ef} \tag{12}$$

3.2.2. Stiffness diagram

The analytical formulations of the failure modes allowed the establishment of the maximum load in tension and compression for the reference model. The ultimate load defined for tension is the minimum between the load calculated for sliding, tie fracture and combined sliding and cone failure. The ultimate load defined for compression is the minimum between the piercing and expulsion of the mortar failure load, combined sliding/failure load and the buckling load.

The remaining parameters needed to define the constitutive model of the spring are: (a) loading/unloading stiffness (K); (b) maximum displacement before strength degradation (d_u); and (c) residual strength of the tie. The loading/unloading stiffness and the maximum displacement were assumed based on the experimental results. In the case of the residual strength, it was defined as 10% of the maximum load, both in tension and compression. This assumption was initially proposed because a residual strength was observed in the experimental tests. Nevertheless, this can be assumed as 0 to be more conservative. In summary, the necessary parameters to define the constitutive model of the spring are presented in Table 2, based on the results computed in sections 3.2.1.1-3.2.1.6. The ultimate load defining the tension behavior

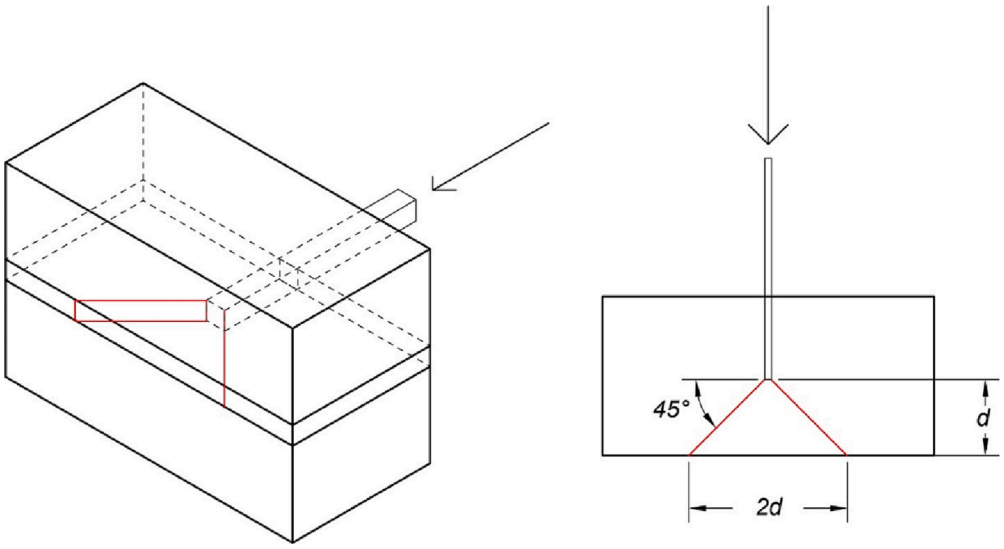

Fig. 8. Idealized mortar failure cone within the mortar joint.

correspond to the combined sliding and cone failure mode, while the ultimate load defining the compression behavior correspond to the buckling load.

Fig. 9 shows the comparison between the simplified force–displacement diagram obtained from the analytical formulas with both the experimental and finite element numerical results. It can be observed that the correspondence between the simplified diagrams and experimental curves is acceptable in terms of maximum load. This is also true in terms of maximum displacement and stiffness, which were experimentally calibrated.

Finally, it should be noted that all values that are here calibrated with the experimental results, namely maximum shear stress at the interface (τ_{max}), loading/unloading stiffness (K) and maximum displacement before strength degradation (d_u), should be provided by the tie manufacturer and specified in technical sheets.

4. Parametric analysis: spring model validation

The simplified spring model was further validated using all experimental results. It is noted that the parameters calibrated experimentally (stiffness and maximum displacement) were kept constant for all analyses. Note also that the experimental results are displayed in black and the spring model stiffness diagrams are displayed in red in the following figures.

Fig. 10 shows the comparison between the numerical force–displacement diagrams obtained by varying the type of tie and the experimental results. The experimental results showed a great dispersion but the simplified spring model diagrams are able to capture well the differences between the different ties, in overall terms, particularly in compression (note that stiffness diagrams for T3 and T4 are superposed).

However, there are some discrepancies. For the two ties that have twisted ends (T3) or end in a hook shape (T4), the failure mode is due to piercing and expulsion of the mortar instead of sliding. As a result, the ultimate load considered for these two tie types is the minimum between the load calculated for piercing and expulsion of the mortar failure, tie fracture and combined sliding and cone failure. The idea is that the hook and twisted ends will avoid a simple sliding mechanism and activate a bigger area of mortar, leading to a cone type failure mode, similar to what happens in compression. The maximum load is relatively close to the experimental results, but underestimated by 20% and 40% for T3 and T4, respectively. Note that stiffness diagrams for T3, T4 and T5 in tension are superposed. On the other hand, the maximum load estimated for T2 and T5 is overestimated by 40% and 60%, respectively.

Table 2
Parameters needed to define the spring model behavior.

Tension		Compression	
$f_{t,max}$ (kN)	2.68	$f_{c,max}$ (kN)	2.57
$f_{t,res}$ (kN)	0.27	$f_{c,res}$ (kN)	0.26
$K_{t,loading}$ (kN/m)	1000	$K_{c,loading}$ (kN/m)	1500
$K_{t,unloading}$ (kN/m)	400	$K_{c,unloading}$ (kN/m)	400
$d_{t,u}$ (mm)	6	$d_{c,u}$ (mm)	5

To further explore the adequacy of the proposed model, results were compared with the experimental parametric study reported in [22], which varied the construction details in some of the assemblages. Fig. 11 shows the force–displacement diagrams obtained varying several parameters of the assemblage but keeping T1 as the tie. In this case, the parameters under analysis included: (i) the type of mortar, varying between M5, M10 and M10 with compressive strength of 5.2 MPa (reference); and (ii) the embedment length, varying betwen 65 mm (reference) and 85 mm. The results for T1-M5 are very similar to the reference model (note that the mortar compressive strength is very similar in both cases). Indeed, the two force–displacement diagrams prepared for T1 and T1-M5 are superposed with minimum differences in tension and larger in compression (40% underestimation of the load). However, when varying the embedment length, the capacity in the experimental test increases notably. This was not expected because it exceeds even the tie fracture maximum load and this effect could not be captured by the spring model.

The diagrams shown in Fig. 12 allow to analyze the influence of several parameters in the mechanical behavior of the masonry assemblage. T2 is the tie used in all cases. The varying parameters included: (i) the type of mortar, varying between M5, M10 and M10 with compressive strength of 5.2 MPa (reference); (ii) the embedment length, varying between 45 mm, 65 mm (reference) and 85 mm; and (iii) the cavity thickness, varying between 75 mm and 100 mm (reference). The results in tension are overall well captured in all cases and the failure is dominated by the sliding of the tie (which has a corrugated shape but does not have twisted ends or hooks). The simplified numerical approach underestimates the peak load by 40% of the load for a smaller embedment length of 45 mm (*T2-45-M10*), and overestimates the peak load by 40% when the mortar is of class M5 (*T2-M5*). In compression, the spring model takes into account the piercing and expulsion of the mortar failure (dominant failure mode) and the results match reasonably well with the experimental results. Nevertheless, the load is significantly

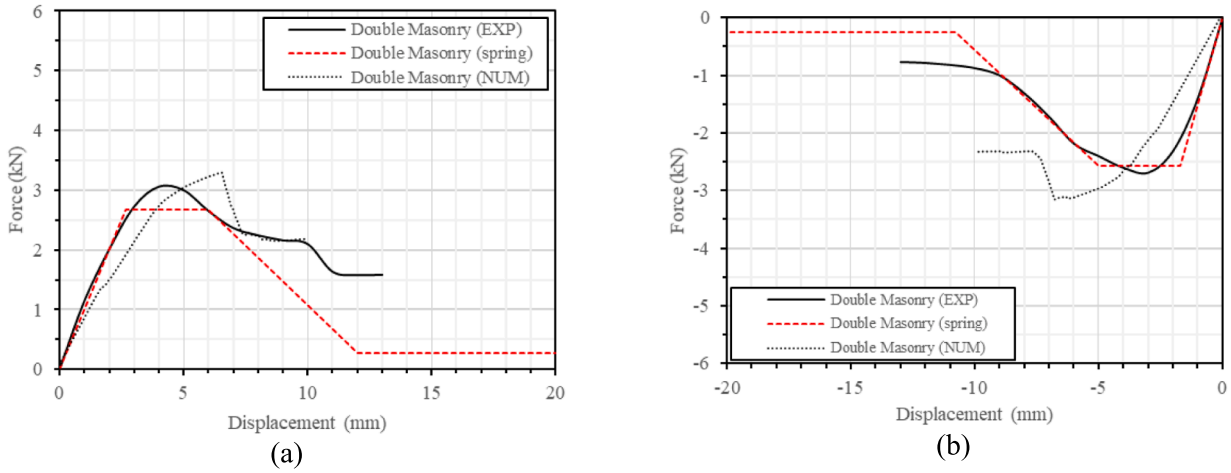

Fig. 9. Comparison between experimental curves, numerical curves and spring stiffness diagram in: (a) tension; and (b) compression.

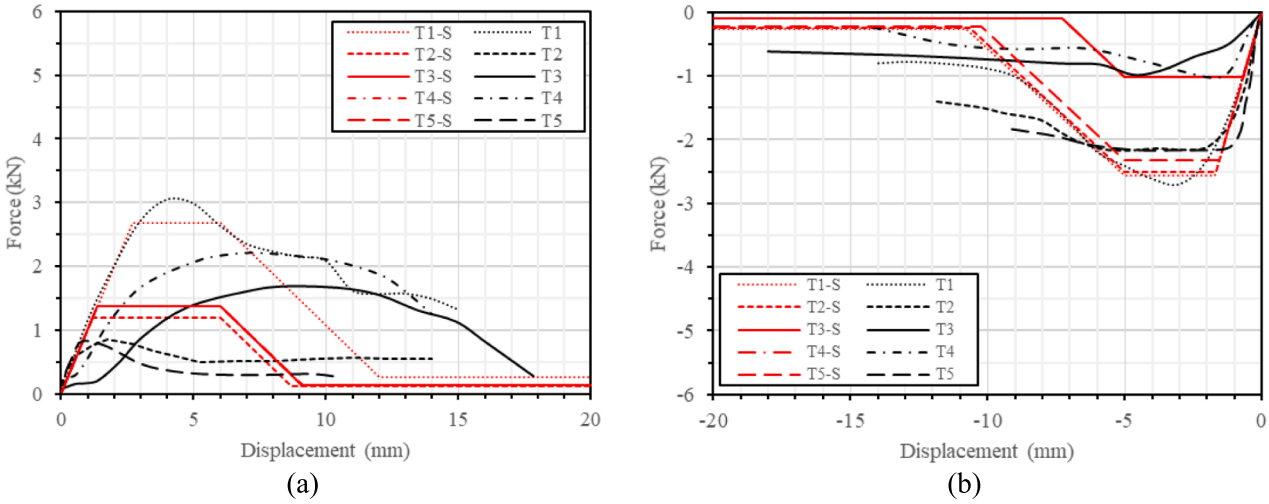

Fig. 10. Comparison between experimental curves and simplified spring model diagrams varying the type of tie in: (a) tension; and (b) compression.

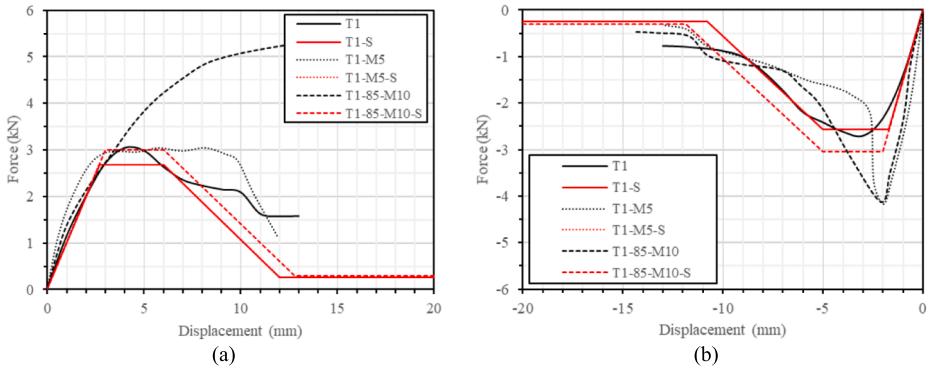

Fig. 11. Comparison between experimental curves and spring stiffness diagrams varying different parameters and using T1 as the type of tie, in: (a) tension; and (b) compression.

underestimated for the two cases that reached high load capacity, which are the ones with a shorter cavity length that helps to avoid the buckling failure.

The simplified numerical approach was also used for analyzing assemblages built with tie T3 (Fig. 13) and varying the following parameters: (i) the type of mortar, varying between M5 and M10; (ii) the embedment length, varying between 45 mm, 65 mm (reference) and 85 mm; and (iii) the cavity thickness, varying between 75 mm and 100 mm

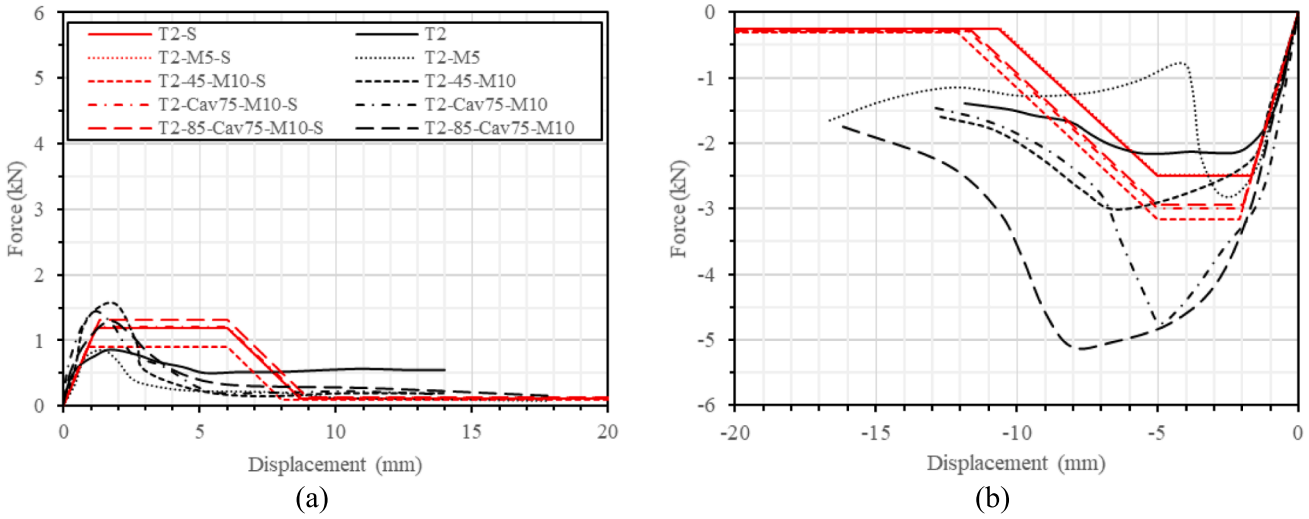

Fig. 12. Comparison between experimental curves and spring stiffness diagrams varying different parameters and using T2 as the type of tie, in: (a) tension; and (b) compression (note that legend is the same as in tension).

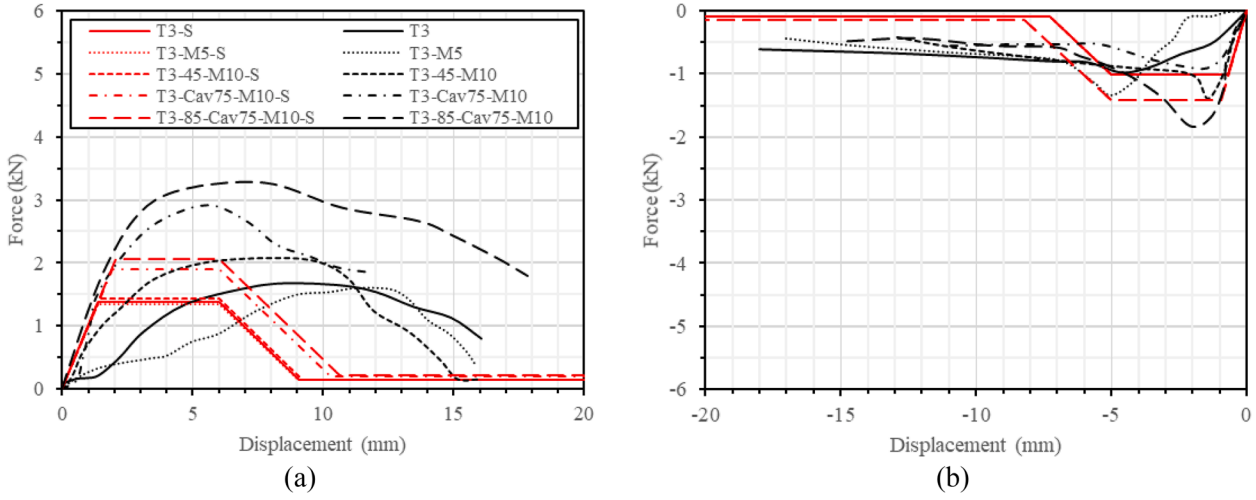

Fig. 13. Comparison between experimental curves and spring stiffness diagrams varying different parameters and using T3 as the type of tie, in: (a) tension; and (b) compression (note that legend is the same as in tension).

(reference thickness), using different combinations. The predominant failure mode in tension is the cone failure. The numerical model tends to underestimate the capacity of the system (around 35% for the two cases with a cavity thickness of 75 mm). The underestimation may be due to the fact that the variation of the shear strength of the brick–mortar interface is neglected and kept the same as the one adopted for the reference model. Nevertheless, models are considered to match well the experimental results and follow well the trends observed. In compression, the model also captures well the experimental behavior of the tie and the overall trend, which is governed by the failure buckling load. Variations are lower than 25% for all cases (always underestimating the maximum load), except for the case with cavity thickness equal to 75 mm (*T3-Cav75-M10*). In this case, the model leads to an overestimation of 50% of the experimental load.

Finally, Fig. 14 shows the diagrams prepared varying several parameters of the assemblage keeping T4 as the tie. The parameters varied included: (i) the type of mortar, varying between M5 and M10; (ii) the embedment length, varying between 45 mm, 65 mm (reference) and 85 mm; and (iii) the cavity thickness, varying between 75 mm and 100 mm (reference thickness), using different combinations. In this case, the results are very similar to the ones obtained in the assemblages built with tie T3. The cone failure type caused by the hook shape controls the capacity in tension and the loads are relatively close to the ones obtained experimentally, but they are systematically underestimated (around 30% of the experimental load). In compression, the loads also match the experimental ones reasonably well and follow well the trends observed experimentally, with variations lower than 25% for all cases.

In summary, the proposed spring model is considered to simulate well the structural behavior of the assemblage under tension and compression loading. Despite the important simplifications assumed, it is able to match well the experimental results in terms of maximum load and the observed response trends. Greater discrepancies result in an underestimation of the load, which can be considered acceptable for design purposes. The simplified approach is thus considered validated and able to simulate the behavior of the tension and compression behavior of tie connections in masonry veneer walls. It should be noted that some of the parameters (e.g. maximum shear stress or stiffness of the embedded tie-mortar connection), which are necessary to define the model, would need to be provided by the tie manufacturers after laboratory testing. Nevertheless, this would be necessary for any modeling

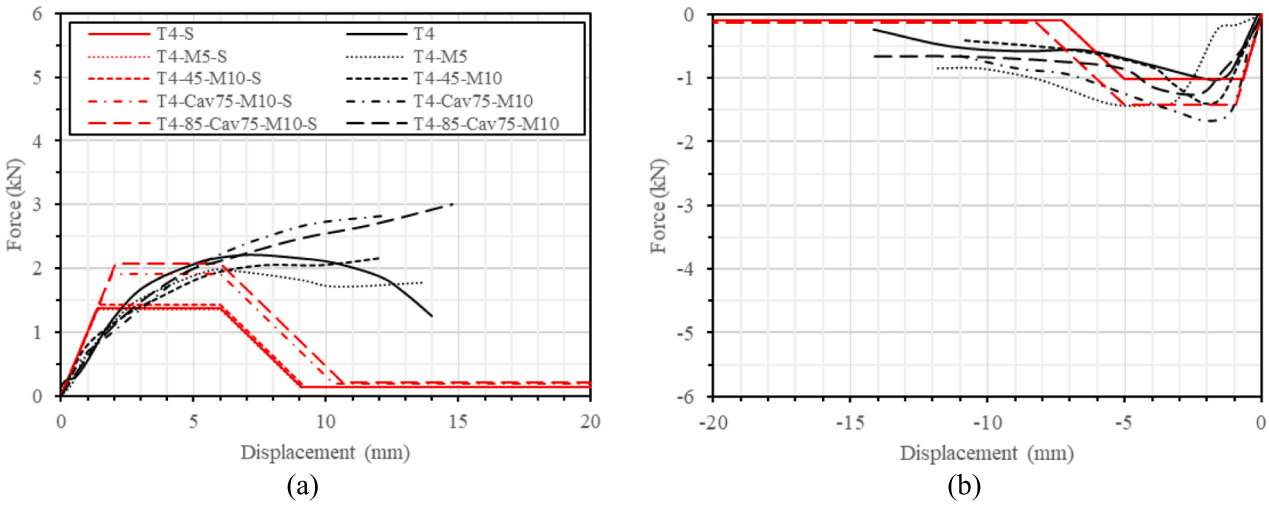

Fig. 14. Comparison between experimental curves and spring stiffness diagrams varying different parameters and using T4 as the type of tie, in: (a) tension; and (b) compression.

strategy that is selected to model this type of tie connection. The simplified approach is particularly oriented for practice since it is a fast approach that can also be easily implemented in more complicated numerical models, e.g. models representing a whole building.

5. Load eccentricity due to the misalignment of mortar joints

One problem that is observed in practice is the probable misalignment of the mortar joints during the construction of veneer walls with brick masonry infill walls. Common solutions in the market to overcome this difficult consist of a vertical channel that allows the tie to be placed at different heights for the interior and the exterior masonry wall, according to the position of the joints of the two masonry leaves (Fig. 15 left). Analyses carried out based on this solution, confirm that such misalignment (and subsequent eccentricity in the application of the load) has a significant influence on the capacity of the tie solution under tension loading.

A preliminary numerical assessment was carried out to better understand the effect of the existing solutions on the structural capacity of the system. The analysis was made following the numerical approach discussed in [33]. Several numerical models were prepared, using the common solution available in the market and varying the level of eccentricity, i.e., the position of the tie within the vertical steel channel (Fig. 15). An interface element with no tension capacity (the normal stiffness of the interface is reduced to zero, when the interface is opening) and no shear stiffness was applied between the vertical steel channel and the brick. A extremely high normal stiffness is assumed in compression so that the channel is able to transmit all the compression load to the brick with no deformation (avoiding interpenetration).

Fig. 15 shows the model and interface with the expected behavior. The interface opens due to the moment induced by the eccentric tension load, but the part under compression does not penetrate into the brick. At the end of the analysis, all the interface is fully open. Fig. 16 shows the numerical load–displacement curves obtained from the analyses. The results show an increasing decrease in the capacity of the tie when increasing the eccentricity.

Fig. 17 shows a diagram of the forces acting when this solution is adopted. Under tension loading (F), the system behaves as a lever, increasing the load acting on the tie (T) because of the hinge that forms at the end of the channel (H). By equilibrium of moments, T can be computed as:

$$T = F\left(\frac{L}{L_2}\right) \tag{13}$$

This equation shows clearly how T increases with increasing eccentricity (e) between the ties. This effect does not occur under compression loading because the channel leans attached to one of the masonry leaves. The channel can separate and bend under tension (no tension or shear capacity), but cannot bend under compression. It is able to transmit all the compression load to the internal masonry wall with no deformation (it does not interpenetrate).

The proposed simplified spring model discussed in section 3 can also be applied for the proposed solution. Simply by using Eq. (13), the reduced capacity of the tie with respect to the reference models (no

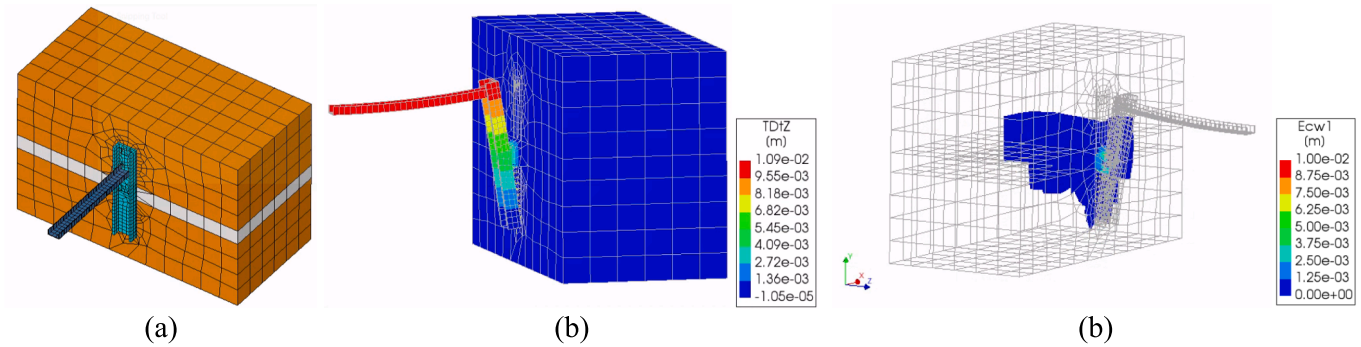

Fig. 15. Numerical model of the construction solution with varying levels of eccentricity of the tie (a); and results at the end of the analysis: displacements (b); and damage in terms of crack width (c).

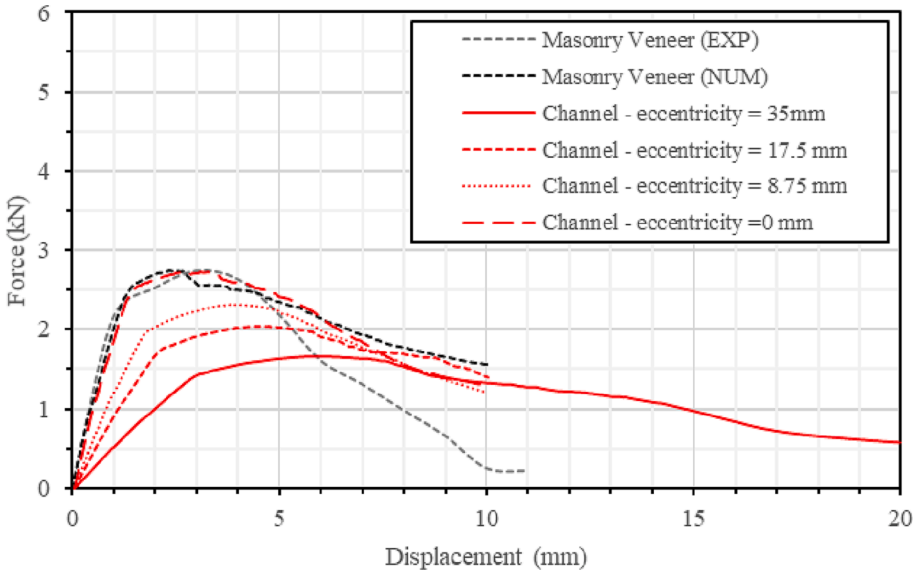

Fig. 16. Comparison between numerical curves for different values of eccentricity.

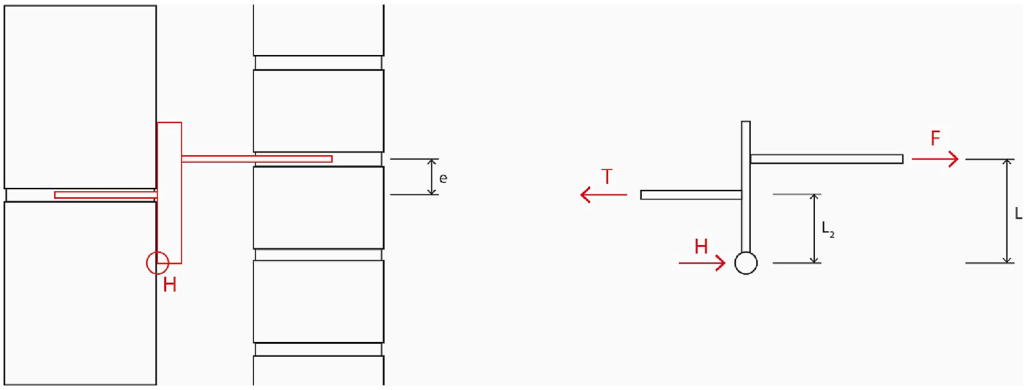

Fig. 17. (left) Available commercial solution to solve the misalignment of mortar joints; and (right) diagram of forces acting on the constructive solution under tension loading.

channel) can be computed. The factor L/L_2 can be used as a reducing factor to compute the ultimate load defined for tension. For example, for different values of eccentricity (e), namely 10, 20 and 35 mm, and assuming a height of the vertical channel of 90 mm ($L_2 = 45$ mm), $f_{t,\max}$ results in 2.2, 1.86 and 1.51 kN, respectively. The reference $f_{t,\max}$ (Table 2) with no eccentricity is 2.68 kN. These results are equivalent to the ones obtained from the numerical analyses shown in Fig. 16.

The results show that the solution observed in the market has a significant influence in the behavior and capacity of the system. The reduction of the capacity should be taken into account in the computation of the maximum capacity if this system is used. Conversely, other solutions can be explored aiming to minimize the eccentricity and solve the construction issue without reducing the capacity of the system.

A possible solution consists of enlarging the vertical channel so that two ties can fit inside (Fig. 18). The separation of the two ties can be established based on the height of the veneer brick (the separation between horizontal joints). The out-of-plane loading would thus be applied on both ties, avoiding the eccentricity in the application of the load. Such system could avoid the reduction of the capacity of the system. It is noted that the idea is that the horizontal bar inserted in the infill masonry is fixed, whereas the two opposite bars embedded within the veneer masonry can be adjusted along the height of the vertical channel, adapting them to the height of the veneer brick and the misalignment with respect to the infill masonry joint.

The proposed solution was also modeled using the approach previously discussed (Fig. 19a). The results show that the use of such solution avoids the reduction of the capacity of the system (Fig. 19b). The maximum load attained by all models is practically the same and the main variation is in the global stiffness of the system, which, as expected, is more flexible due to the bending of the vertical channel. However, the channel can be designed to be stiffer if needed to limit the damage in the masonry.

The main variation is that the system would become more flexible due to the bending of the vertical channel, which should be taken into consideration in its design by the manufacturer and should be specified in technical sheets. Moreover, the failure of the vertical channel element should be also evaluated, particularly under bending and shear. Similar to the formula proposed to analyze the possible tie fracture (Eq. (1), the formulas proposed by the Eurocode 3 [15] to evaluate the resisting bending moment (M_{max}) and shear strength (V_{max}) can be applied:

$$M_{max} = Wf_y \tag{14}$$

$$V_{max} = A_V(f_y/\sqrt{3}) \tag{15}$$

where M_{max} is the maximum bending moment that the tie can withstand, W is the section modulus, f_y is the yield strength, V_{max} is the maximum shear force that the tie can withstand, and A_V is the shear area.

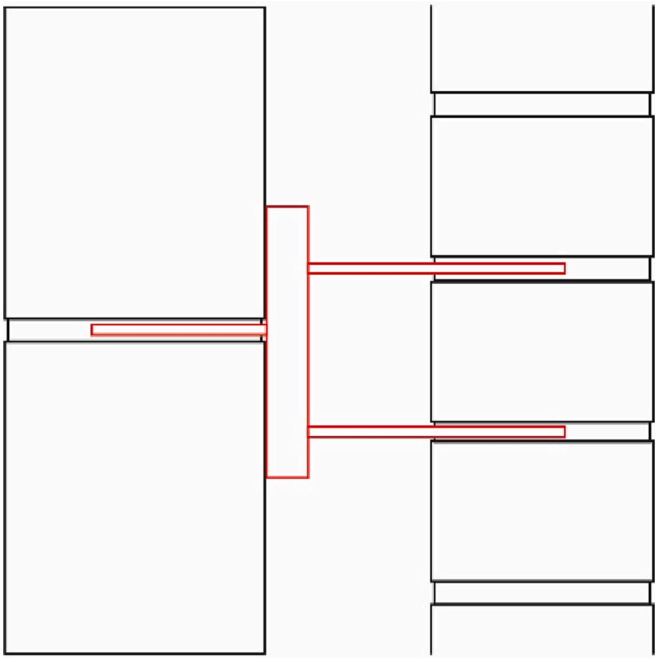

Fig. 18. Proposal to solve the misalignment of mortar joints.

6. Conclusions

Steel ties are the most common device to structurally connect veneer walls to the main structural system and are responsible for transferring both in-plane and out-of-plane loads that can occur, for example, under seismic and wind loading. The main objective of the present paper was to develop and propose a simplified spring model with nonlinear elasticity defined by distinct loading and unloading stiffness diagrams. The simplified model is ready and particularly oriented for practice, so that practitioners can use it to assess the structural performance of the ties under out-of-plane loading. One limitation of the proposed simplified modeling approach with nonlinear elasticity is that it does not take into account the pinching effect, assuming plastic unloading. Thus, the simplified modeling approach is mainly recommended for nonlinear static analysis, aiming to avoid a non-conservative assessment after the analysis due to an overprediction of the energy dissipated by the ties in the case of nonlinear dynamic analyses. The model can be extended in the future with a more appropriate hysteretic model that can also take into account the pinching effect.

Nevertheless, the proposed model is kept simple and can be easily implemented in more complicated numerical models for design purposes. This can be particularly helpful because estimating the load acting on each tie for complex buildings and various loading conditions is difficult. The use of the proposed simplified spring model on numerical analyses of greater scale allows to estimate the load acting on each tie more precisely. Thus, the position and amount do not need to be designed for maximum loading, e.g. reducing the amount of ties at the base of the building, where the seismic loading is lower than at the top, optimizing the structural design.

The simplified model consists of six simple analytical formulations that are used to compute the maximum load that the tie can stand according to the most common failure modes observed during the tension–compression tests performed on ties connecting brick masonry veneers with brick masonry infill walls. The location of the ties considered in the present study is the mortar joint. Thus, the proposed model is validated for this configuration. In the future, other relevant failure modes for different tie locations, e.g., masonry unit pull-out for ties embedded in masonry units, can be considered to extend the scope of the proposed model. The ultimate load defined for tension and compression is the minimum computed between the different failure modes considered. The remaining parameters necessary to define the spring stiffness diagrams are the loading/unloading stiffness and maximum displacement before strength degradation. These parameters, as well as other key material parameters, namely maximum shear stress at the tie-mortar interface, should be provided by the tie manufacturer.

The model was validated with experimental results available for ties of different geometries and different construction details (e.g. mortar characteristics or tie embedment length). Despite the simplifications assumed, it is able to match well the experimental results in terms of the overall trend. Variations are overall lower than 25% in both tension and compression, but there are some differences over 40%. Some differences may be attributed to the use of non-calibrated material parameters for all models, e.g., the shear strength of the brick–mortar interface, which may vary among the different ties. Nevertheless, greater discrepancies result in an underestimation of the load, which can be considered acceptable for design purposes.

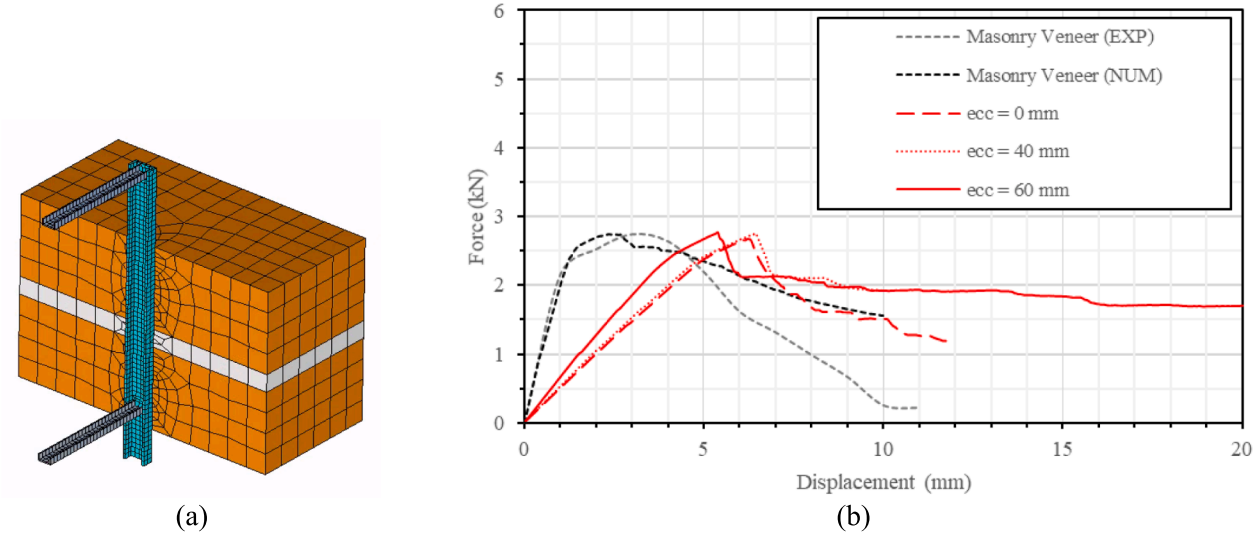

Fig. 19. (a) Numerical model prepared with the proposed solution; and (b) comparison between numerical curves for different values of eccentricity according to the position of the ties in the proposed solution.

Finally, the paper addresses a common construction problem typically encountered during the construction of masonry veneer walls, namely the probable misalignment of the horizontal joints of the veneer and infill masonry walls. An existing solution consisting of a vertical channel that allows one tie to be placed at different heights was analyzed, showing that it is not structurally appropriate because it can significantly reduce the capacity of the system due to the eccentricity in the application of the load. Thus, a new solution, adapted from the existing solution but composed of two adjustable horizontal ties is proposed. The new solution is able to solve the misalignment without reducing the capacity of the tie and should be preferred. In any case, the paper proposes simple formulations to consider the reduction of the capacity of the system in the case of adopting the existing solution, as well as formulations to compute the possible failure of the vertical channel due to bending and shear.

Declaration of Competing Interest

The authors declare that they have no known competing financial interests or personal relationships that could have appeared to influence the work reported in this paper.

Acknowledgments

The authors acknowledge the support of the Portuguese Foundation for Science and Technology (FCT), through the financing of the research project SEVen – Development of Sustainable Ceramic Brick Masonry Veneer Walls for Building Envelops (PTDC/ECI-CON/30876/2017).

References

[1] AFNOR (2008) NF DTU 20.1 in P1-1. Ouvrages en maçonnerie de petits éléments – Parois et murs; Partie 1-1: Cahier des clauses techniques types: France.
[2] Akhoundi F. Strategies for Seismic Strengthening of Masonry Infilled Reinforced Concrete Frames. Guimarães, Portugal: Universidade do Minho; 2016. Ph.D. Thesis.
[3] Akhoundi F, Vasconcelos G, Lourenco P, Silva L, Cunha F, Fangueiro R. In-plane behavior of cavity masonry infills and strengthening with textile reinforced mortar. Eng Struct 2018;156:145–60.
[4] Ancon. Wall ties & Restraints Fixings for the construction industry. Sheffield, United Kingdom: Ancon Building Products; 2016.
[5] Arslan O, Messali F, Smyrou E, Bal İE, Rots JG. Experimental characterization of the axial behavior of traditional masonry wall metal tie connections in cavity walls. Constr Build Mater 2021;266:121141.
[6] Arslan O, Messali F, Smyrou E, Bal İE, Rots JG. Mechanical modelling of the axial behaviour of traditional masonry wall metal tie connections in cavity walls. Constr Build Mater 2021;310:125205.
[7] BIA. Technical Notes on Brick Construction 44B: Wall Ties for Brick Masonry. Reston, VA, USA: Brick Industry Association (BIA); 2003.
[8] BIA. Technical Notes on Brick Construction 28: Brick Veneer Wood Stud Walls. Reston, VA, USA: Brick Industry Association (BIA); 2012.
[9] BSI. BS 5628: Code of practice for the use of masonry. UK: British Standards Institution (BSI); 2005.
[10] Burton C, Visintin P, Griffith M, Vaculik J. Laboratory investigation of pull-out capacity of chemical anchors in individual new and vintage masonry units under quasi-static, cyclic and impact load. Structures 2021;34:901–30.
[11] Ceci AM, Contento A, Fanale L, Galeota D, Gattuli V, Lepidi M, et al. Structural performance of the historic and moderns buildings of the University of ĹAquila during the seismic events of April 2009. Eng Struct 2010;32:1899–924.
[12] Contrafatto L, Cosenza R. Prediction of the pull-out strength of chemical anchors in natural stone. Frattura ed Integrità Struturalle 2014;29:196–208.
[13] Cook RA, Doerr GT, Klingner RE. Bond stress model for design adhesive anchors. ACI Struct J 1993;90:514–24.
[14] Eligehausen R, Mallée R, Rehm G. Befestigungen mit Verbundankern. Betomverk + Fertigteil Technik 1985;10:686–92.
[15] EN 1993-1-1 (2005) Eurocode 3: Design of steel structures – Part 1-1: General rules and rules for buildings, European Committee for Standardization (CEN): Brussels, Belgium, 2005.
[16] EN 1996-1-1 (2005) Eurocode 6: Design of masonry structures - Part 1-1: General rules for reinforced and unreinforced masonry structures, European Committee for Standardization (CEN): Brussels, Belgium.
[17] Giresini L, Puppio ML, Taddei F. Experimental pull-out tests and design indications for strength anchors installed in masonry walls. Mater Struct 2020;53:103.
[18] Jo S. Seismic Behavior and Design of Low-rise Reinforced Concrete Masonry with Clay Masonry Veneer. Austin, USA: University of Texas; 2010. Ph.D. Thesis.
[19] Klingner RE, Shing PB, McGinley WM, McLean DI, Okail H, Jo S, et al. Seismic performance tests of masonry and masonry veneer. J ASTM Int 2010;7(3):102740.
[20] Magenes, G., Bracchi, S., Graziotti, F., Mandirola, M., Manzini, C. F., Morandi, P., Palmieri, M., Penna, A., Rosti, A., Rota, M., Tondelli, M. (2008) Preliminary damage survey to masonry structures after the May 2012 Emilia earthquakes, v.1.
[21] Martins A, Vasconcelos G, Costa AC. (2014) Comportamento sísmico de paredes de alvenaria de fachada - uma breve revisão. In Proc. of JPEE- Jornadas Portuguesas de Engenharia de Estruturas, Lisboa, Portugal.
[22] Martins A. Seismic Behaviour of Masonry Veneer Walls. Portugal: Universidade do Minho, Guimarães; 2018. Ph.D. Thesis.
[23] McVay M, Cook RA, Krishnamurthy K. Pullout simulation of postinstalled chemically bonded anchors. J Struct Eng 1983;122(9):1016–24.
[24] Memari AM, Burnett EFP, Kozy BM. Seismic response of a new type of masonry tie used in brick veneer walls. Constr Build Mater 2002;16(7):397–407.
[25] Mendes F. Durabilidade de fachadas. M.Sc. Thesis. Portugal: Universidade do Porto; 2009.
[26] Mendonça P. Habitar sob uma segunda pele. Portugal: Universidade do Minho; 2005. Ph.D. Thesis.
[27] MSJC (2008) Building Code Requirements for Masonry Structures (TMS 402-08/ ACI 530-08/ASCE 5-08. Masonry Standards Joint Committee (MSJC), American Society of Civil Engineers, The Masonry Society and American Concrete Institute: Reston, VA, USA.
[28] MSJC (2008) Specification for Masonry Structures (TMS 602-08/ACI 530.1-08/ ASCE 6-08). Masonry Standards Joint Committee (MSJC), American Society of Civil Engineers, The Masonry Society and American Concrete Institute: Reston, VA, USA.
[29] Muhit IB, Masia MJ, Stewart MG, Isfeld AC. Spatial variability and stochastic finite element model of unreinforced masonry veneer wall system under Out-of-plane loading. Eng Struct 2022;267:114674.
[30] Muhit IB, Masia MJ, Stewart MG. Monte-Carlo laboratory testing of unreinforced masonry veneer wall system under out-of-plane loading. Constr Build Mater 2022; 321:126334.
[31] Muhit IB, Stewart MG, Masia MJ. Probabilistic constitutive law for masonry veneer wall ties. Aust J Struct Eng 2022;23(2):97–118.
[32] Okail H. Experimental and analytical investigation of the seismic performance of low-rise masonry veneer buildings. San Diego, USA: University of California; 2010. Ph.D. Thesis.
[33] Ortega J, Mendes N, Vasconcelos G. Numerical simulation of the tension-compression behavior of tie connections in brick masonry walls. CivilEng 2022;3 (2):441–55.
[34] Pereira P, Aguiar JB, Camões A, Lourenço PB. (2010) The Portuguese masonry's mechanical characterization. In Proc. of the 8th International Masonry Conference 2010, Dresden, Germany.
[35] Pereira MFP, Pereira MFN, Ferreira JED, Lourenço PB. (2011) Behavior of masonry infill panels in RC frames subjected to in-plane and out-of-plane loads. In Proc. of the 7th International Conference AMCM 2011: Analytical and New Concepts In Concrete and Masonry Structures, Krakow, Poland.
[36] Ramirez R, Muñoz R, Lourenço PB. (2023) On Mechanical Behavior of Metal Anchors in Historical Brick Masonry: Testing and Analytical Validation. Applied Sciences, 13(6), 3999.
[37] Reneckis D, LaFave JM (2009) Seismic Performance of Anchored Brick Veneer, Report No. NSEL-016, Newmark Structural Laboratory Report Series, University of Illinois at Urbana-Champaign: USA.
[38] TNO (2021) DIsplacement method ANalizer Finite Element Analysis (DIANA FEA) Documentation. Release 10.5, DIANA FEA BV: Delft, The Netherlands.
[39] Zisi N. The influence of brick veneer on racking behavior of light frame wood shear walls. Knoxville, USA: University of Tennessee; 2009. Ph.D. Thesis.